Complexes of $XeHXe^+$ with Simple Ligands: A Theoretical Investigation on $(XeHXe^+)L$ (L = N_2, CO, H_2O, NH_3)

Stefano Borocci, Maria Giordani, and Felice Grandinetti*

Dipartimento per la Innovazione nei sistemi Biologici, Agroalimentari e Forestali (DIBAF), Università della Tuscia, L.go dell'Università, s.n.c., 01100 Viterbo (Italy)

Dedicated to Prof. Markku Räsänen on the occasion of his 65th birthday

ABSTRACT: The structure, stability, and harmonic frequencies of the ($XeHXe^+$)L complexes (L = N_2, CO, H_2O, NH_3) were investigated by *ab initio* and density functional theory (DFT) calculations. Their bonding situation was also assayed by Natural Bond Orbital (NBO), Atoms-in-Molecules (AIM), and Energy Decomposition (EDA) analyses. For any L, we located a linear and a T-shaped isomer, whose energy difference progressively increases in the order N_2 < CO < H_2O < NH_3, and ranges from nearly 0 to 4.5 kcal mol^{-1}. The absolute complexation energies of both the linear and the T-shaped isomers also increase in the same order, and their EDA analysis revealed the prevailing contribution of electrostatic interactions. The non-covalent character of the bonding between $XeHXe^+$ and L was confirmed by the AIM analysis. In particular, we based on the joint use of numerical AIM indices, and graphic examination of the local Hamiltonian kinetic energy density, $K(\boldsymbol{r})$. Interestingly, this function visually signs the "covalent" regions occupied by $XeHXe^+$ and L, and the "non-covalent" zones existing between them, which include, in particular, the bond critical point located on the Xe-L bond paths. Only for the linear ($XeHXe^+$)NH_3, the AIM analysis suggested an onset of covalency in the xenon-nitrogen interaction. Further work is in progress to examine the effectiveness of $K(\boldsymbol{r})$, and its plotted forms, as a signing function of the bonding situation of noble-gas compounds.

Keywords: AIM and NBO Analysis - Hamiltonian kinetic energy density - Noble Gases - Theoretical Calculations - Xenon Cations

1. INTRODUCTION

The chemistry of the noble gases is currently enjoying fascinated interest, stimulated also by some noticeable, and somewhat unexpected advances achieved in the last two decades.[1-4] Particularly relevant in this regard was the contribution of the Helsinki's group, who discovered an entire new family of noble gas molecules.[5-8] These species have general formula HNgY (Ng = noble gas atom; Y = electronegative fragment), and are obtained by photodissociation of HY in a cold Ng matrix. Observed molecules include HArF, a first (and to date unique) neutral argon compound,[9] more than twenty HKrY and HXeY,[5-8] and the dinuclear HXeCCXeH,[10] and HXeOXeH.[11] Non-hydrogen species such as ClXeCN and BrXeCN were also detected.[12] Interestingly, in the cold environment of the solid matrices it is also possible to trap noble-gas ions, including, in particular, the most extensively investigated $NgHNg^+$ (Ng = Ar, Kr. Xe). These species are simplest benchmark cases of solvated ions, and, over the years, they have attracted sustained experimental and theoretical interest.[13-41] The $NgHNg^+$ are produced by UV photolysis of hydrogenated molecules, by deposition through discharge, and by fast-electron irradiation.[13,18,20,21,23,32] They possess a linear, centrosymmetric structure ($D_{\infty h}$),[14,24,26,34,37] and are identified by their characteristic ν_3 infrared (IR) absorption, and intense $\nu_3 + n\nu_1$ (n = 1 - 4) combination progression, that arises from the strong coupling of the two modes.[21,23] The investigation of these vibrational patterns,[22,24-26,33,37,38] and the mechanisms of the annealing-induced decay processes[15-17,30,31] are indeed major themes in the chemistry of the $NgHNg^+$. Over the years, the interest was also extended to the mixed ions $ArHKr^+$, $ArHXe^+$, and $KrHXe^+$.[26,27,32,33]

The $NgHNg^+$ are covalently bound, and it becomes of interest to speculate on their conceivable behavior as core units of larger complexes. The interaction with additional Ng atoms was indeed investigated by various theoretical methods,[13,34-36,39] but the complexes of the $NgHNg^+$ with molecular ligands (L) have to date received only little attention. The only available evidence is the study performed in 2006 by Lignell et al.,[42] who studied the interaction of $ArHAr^+$ and $KrHKr^+$ with molecular nitrogen, and unraveled the formation of the singly-coordinated $(NgHNg^+)N_2$ (Ng = Ar, Kr). The calculations revealed two conceivable isomers, namely a linear structure with N_2 coordinated to one of the Ng atoms, and a T-shaped structure with N_2 coordinated to the H atom. The latter was predicted to be slightly more stable, but the IR experiments pointed to the exclusive formation of the linear complex. It was thus speculated that the T-shaped structure did not fit the vacancies of the Ng lattice.[42] In general, the stability of homologue noble-gas compounds tends to increase moving down in the group. Thus, the ascertained existence of $(ArHAr^+)N_2$ and $(KrHKr^+)N_2$ suggests the conceivable stability of $(XeHXe^+)N_2$, and hints also to a probably large class of $(XeHXe^+)L$. This expectation was confirmed by the present calculations, that revealed, in particular, the stability of the complexes of $XeHXe^+$ with the exemplary ligands N_2, CO, H_2O, and NH_3. The structure and bonding properties of these ions will be discussed in the present article.

2. COMPUTATIONAL DETAILS

The *ab initio* calculations were performed with the Gaussian 03.[43] The employed methods were the second-order Møller-Plesset (MP2)[44] and the coupled cluster with inclusion of single and double substitutions and an estimate of connected triples, CCSD(T).[45] The Xe atom was treated by the small-core (28 electrons), scalar-relativistic effective core potential (ECP-28) developed by the Stuttgart/Cologne group,[46] and the employed basis set was the aug-cc-pVTZ-PP, obtained combining the Dunning's correlation consistent triple-zeta basis sets for H, C, N, and O,[47] with the (13*s*12*p*10*d*2*f*)/[6*s*5*p*4*d*2*f*] basis designed for Xe in conjunction with the ECP-28.[46] Both the MP2 and the CCSD(T) were employed within the frozen-core approximation (the frozen-core orbitals of Xe were 4*s*4*p*4*d*). The geometry optimizations performed at the MP2 level of theory were based on analytical energy gradients, and any located critical point was characterized as an energy minimun or higher-order saddle point by calculating its harmonic frequencies, used also to evaluate the zero-point vibrational energy (ZPE). The dissociation energies calculated at the CCSD(T) level of theory were corrected for the basis set superposition error (BSSE) using the counterpoise method of Boys and Bernardi.[48]

The weights of the resonance structures were evaluated by the natural resonance theory (NRT)[49-51] developed within the framework of the the Natural Bond Orbital (NBO) analysis[52] (all the weighted structures were explicitly chosen as reference structures). These calculations were performed with the GENNBO 6.0W program.[53]

The energy decomposition analysis (EDA) was performed by the extended transition state method developed by Ziegler and Raouk[54-56] in the framework of density

functional theory (DFT), and implemented in the Amsterdam Density Functional (ADF) code.[57-59] The chosen functional was the B3LYP,[60-62] corrected for dispersion by the Grimme's method[63] (B3LYP-D). The MOs were expanded in a large uncontracted set of Slater-type orbitals (STOs)[64] containing diffuse functions. The employed basis set, denoted as TZ2P, is of triple-ζ quality for all atoms and is augmented with two sets of polarization functions, namely, 2*p* and 3*d* on H, 3*d* and 4*f* on C, N, and O, and 5*d* and 4*f* for Xe. An auxiliary set of *s*, *p*, *d*, *f*, and *g* STOs, centered on all nuclei, was used to fit the electron density and to obtain accurate Coulomb potentials in each SCF cycle.[65,66] Relativistic effects were included by the zero-order regular approximation (ZORA).[67]

The Atoms-in-Molecules (AIM)[68] calculations were performed with the AIMAll program.[69] We calculated in particular the charge density $\rho(\boldsymbol{r})$, the Laplacian of the charge density $\nabla^2\rho(\boldsymbol{r})$, the local energy density $H(\boldsymbol{r})$, the local kinetic (Lagrangian) energy density $G(\boldsymbol{r})$, the local potential energy density $V(\boldsymbol{r})$, and the local kinetic (Hamiltonian) energy density $K(\boldsymbol{r})$ at the bond critical points (bcp's), intended as the points on the attractor interaction lines where $\nabla\rho(\boldsymbol{r}) = 0$. The missing core electron density on Xe was modelled by a single *s*-type Gaussian function, with exponent $\alpha = 4\pi$ and coefficient $c = 8\times N_c$ (N_c = number of core electrons = 28). As recently discussed,[70] for small-core pseudopotentials, the inclusion of a single function is in general sufficient to avoid the interference of the spurious electron density critical points which arise from the absence of the core electron density.

3. RESULTS AND DISCUSSION

A. Geometries and NBO Analysis. The MP2/aug-cc-pVTZ-PP optimized geometries of the ($XeHXe^+$)L (L = N_2, CO, H_2O, NH_3) are shown in Figures 1 and 2.

<Figures 1 and 2 near here, please>

The predicted bond distance of $XeHXe^+$, 1.862 Å, is in very good agreement with the CCSD(T)/aug-cc-pVTZ-PP estimate of 1.869 Å, and these values well compare with previous MP2 and CCSD(T) results obtained with different pseudopotentials, basis sets, and numbers of correlated orbitals.[22,24,26-28,41]

Likewise the previously investigated ($ArHAr^+$)N_2 and ($KrHKr^+$)N_2,[42] irrespective of L, we located two distinct ($XeHXe^+$)L energy minima, namely the linear and the T-shaped isomers. The former arise from the coordination of L to one of the Xe atoms of $XeHXe^+$ (henceforth indicated as Xe1, see Figure 1). The Xe1-L distances, are, in general, rather long and range from 3.336 Å for L = CO to 2.829 Å for L = NH_3. In any case, the interaction with the ligand significantly affects the bond distances of $XeHXe^+$, and produces, in particular, the contraction of the Xe1-H bond, and the elongation of the Xe-H bond. These effects both increase in the order N_2 < CO < H_2O < NH_3, and range, respectively, from 0.056 Å to 0.184 Å, and from 0.064 Å to 0.379 Å. In the T-shaped complexes (see Figure 2), the $XeHXe^+$ moiety is bent, with a deviation from linearity that progressively increases in the order N_2 < CO < H_2O < NH_3, and ranges from 2.1° to 8.5°. These structures are symmetric (L = N_2, CO, H_2O) or only slightly asymmetric (L = NH_3), and feature two equivalent or nearly-equivalent Xe-H bonds, whose distances are only slightly different from $XeHXe^+$. Thus, for L = N_2, CO, and H_2O, the Xe-H bond contracts by 0.001 - 0.003 Å, in the hinted trend N_2 < CO < H_2O. For L = NH_3, the

two non-equivalent Xe-H and Xe1-H bonds are, respectively, shorter and longer than $XeHXe^+$ by only 0.012 Å and 0.007 Å. Consistently, the Xe-L bond distance of any T-shaped complex is longer than that of the corresponding linear isomer, with particularly large differences of nearly 0.5 Å - 0.6 Å for $(XeHXe^+)H_2O$ and $(XeHXe^+)NH_3$.

In general, the linear, centrosymmetric $Xe\text{-}H\text{-}Xe^+$ can be viewed as a three centers-four electrons species,[71,72] best described by the two equivalent resonance structures $(Xe)(H\text{-}Xe^+)$ and $(Xe\text{-}H^+)(Xe)$. In the symmetric or nearly symmetric T-shaped complexes, the two $[(Xe)(H\text{-}Xe^+)]L$ and $[(Xe\text{-}H^+)(Xe)]L$ resonance structures are still expected to be equivalent, or nearly equivalent. On the other hand, in the linear complexes (see Figure 1), the two resonance structures **I** and **II** are in general non equivalent:

$(Xe)(H\text{-}Xe1^+)(L)$ $\qquad$ $(Xe\text{-}H^+)(Xe1)(L)$

I $\qquad$ **II**

In particular, if one assumes that the relative weight of **I** progressively increases in the order $N_2 < CO < H_2O < NH_3$, this explains the progressively increased contraction of Xe1-H, and the concomitant elongation of Xe-H predicted by the geometry optimizations. This suggestion was indeed confirmed by the NRT analysis, which unraveled also quantitative changes in the character and the strength of the Xe1-H and Xe-H bonds. The relevant data are given in Table 1.

<Table 1 near here, please>

For $XeHXe^+$, the NRT predicts the two expected resonance structures of identical weights. The order of the Xe-H bond is 0.5, with a slightly prevailing character of ionic contribution (54.0%). For any linear $(XeHXe^+)L$, the weight of the resonance structure **I**

is instead higher than that of structure **II**, with predicted percentage contributions that increase from 55.5% up to 74.9% passing from N_2, to CO, H_2O, and NH_3. Consistently, the order of the Xe1-H bond progressively increases from 0.555 to 0.749, and the order of the Xe-H bond progressively decreases from 0.431 to 0.190. These variations are accompanied by a parallel increase (from 51.4% to 66.9%) and decrease (from 40.6% to 21.6%), respectively, of the covalent character of these bonds. As for the T-shaped complexes, the NRT analysis (not included in Table 1) confirmed the two expected identical or nearly identical weights of the two resonance structures $[(Xe)(H\text{-}Xe^+)]L$ and $[(Xe\text{-}H^+)(Xe)]L$, with predicted properties of the Xe-H bonds quite close to those of the naked $XeHXe^+$.

The NBO atomic charges of the $(XeHXe^+)L$ (L = N_2, CO, H_2O, NH_3) are given in Table 2.

<Table 2 near here, please>

For the linear species, passing from N_2 to CO, H_2O, and NH_3, q(Xe1) increases from 0.510 *e* to 0.660 *e*, and q(Xe) decreases from 0.395 *e* to 0.186 *e*. These trends are indeed consistent with the progressively increased role of the resonance structure **I**, which features a formally non-bonded, neutral Xe atom, and a formally positively-charged Xe1 atom. It is also of interest to note that the H atom essentially retains the charge of the naked $XeHXe^+$ (nearly 0.1 *e*). One also notes that, while the interaction with the ligand produces an appreciable flux of charge from Xe1 to Xe, there is no appreciable charge transfer from the ligand to $XeHXe^+$. The predicted values of Δq (see Table 2) range in fact from 0.002 *e* to 0.052 *e*, and increase in the order N_2 < CO < H_2O < NH_3. For the T-shaped isomers, this flux of charge is even smaller. We also note here that the NRT analysis did not detect any contribution of direct Xe-L interactions. These findings

are first suggestions that, in both the linear and the T-shaped $(XeHXe^+)L$, the interaction between $XeHXe^+$ and L is prevailingly non covalent (*vide infra*).

B. Stabilities and EDA Analysis. To investigate the energy differences between the linear and the T-shaped $(XeHXe^+)L$ (L = N_2, CO, H_2O, NH_3), and their stabilities with respect to the dissociation

$$(XeHXe^+)L \rightarrow XeHXe^+ + L \qquad (1)$$

we performed single-point CCSD(T)/aug-cc-pVTZ-PP calculations at the MP2/aug-cc-pVTZ-PP optimized geometries. The obtained data are listed in Table 3.

<Table 3 near here, please>

In general, the ΔE_{el} of (1) increases in the order N_2 < CO < H_2O < NH_3, and ranges from 2.8 kcal mol^{-1} to 15.7 kcal mol^{-1} for the linear isomers, and from 2.8 kcal mol^{-1} to 11.2 kcal mol^{-1} for the T-shaped isomers. Therefore, while the linear and T-shaped $(XeHXe^+)N_2$ and $(XeHXe^+)CO$ are degenerate or nearly degenerate, the linear $(XeHXe^+)H_2O$, and $(XeHXe^+)NH_3$ are more stable than their corresponding T-shaped isomers.[73] The inclusion of ZPE and BSSE reduces the absolute binding energies, but does not appreciably alter the relative stabilities of the various isomers. To appreciate the factors which affect the binding energies and stabilities of the $(XeHXe^+)L$, we performed the energy decomposition analysis (EDA) of the interaction between $XeHXe^+$ and L. Within this method,[54-56] assuming the use of a dispersion-corrected functional, the interaction energy between two fragments, ΔE, is split into five terms:

$$\Delta E = \Delta E_{prep} + \Delta E_{elstat} + \Delta E_{Pauli} + \Delta E_{orb} + \Delta E_{disp}$$

ΔE_{prep} (preparation energy) is the energy required to deform the ground-state separated fragments to the geometries that they acquire in the complex. ΔE_{elstat} is the classical electrostatic interaction between the unperturbed charge distributions of the prepared fragments. It is calculated using frozen electron densities, and can be considered as an estimate of the electrostatic or ionic contribution to the binding energy. ΔE_{Pauli} arises when the wave function of the two superimposed fragments is renormalized and antisymmetrized. This contribution is dominated by the increase in the kinetic energy of the electrons, and is typically positive (repulsive). ΔE_{orb} arises when the Kohn-Sham orbitals relax to their final optimal form. It accounts for electron pair bonding and charge transfer, as well as intra-fragment polarization. ΔE_{disp} is calculated as an extra final term, ΔE_{elstat}, ΔE_{Pauli}, and ΔE_{orb} remaining unchanged.

The computational level chosen for the EDA was the B3LYP-D/TZ2P (at the MP2/aug-cc-pVTZ-PP optimized geometries). According to a very recent benchmark study on the performance of various functionals in the EDA analysis of cationic complexes of the noble gases,[74] this computational level is expected to furnish dissociation energies that are quite close to the CCSD(T) estimates. The obtained results, reported in Table 4, indeed confirm this expectation.

<Table 4 near here, please>

The B3LYP-D/TZ2P//MP2/aug-cc-pVTZ-PP estimates of the ΔE_{el} of (1) are, in fact, in very good agreement with the CCSD(T)/aug-cc-pVTZ-PP//MP2/aug-cc-pVTZ-PP values quoted in Table 3, with a mean unsigned deviation of only 0.41 kcal mol^{-1}. More interestingly, it is now possible to appreciate the factors which affect the complexation energies. First, for both the linear and the T-shaped isomers, the order of stabilities with respect to ligand loss (N_2 < CO < H_2O < NH_3) actually reflects the strictly similar trends

of both the repulsive (ΔE_{prep} and ΔE_{Pauli}) and the attractive (ΔE_{elstat}, ΔE_{orb}, and ΔE_{disp}) contributions to the overall interaction. In addition, one learns that the dissociation energies of $(XeHXe^+)H_2O$ and $(XeHXe^+)NH_3$ larger than those of $(XeHXe^+)N_2$ and $(XeHXe^+)CO$ essentially arise from larger contributions of the electrostatic term (ΔE_{elstat}), which in turn reflect the different polarity of the involved ligands. Passing from N_2 and CO to H_2O and NH_3, the ΔE_{orb} term also increases, but to a much lower extent than ΔE_{elstat}. As a matter of fact, for both the linear and the T-shaped $(XeHXe^+)L$, ΔE_{elstat} prevails on ΔE_{orb}, and this is a further suggestion of the essentially non-covalent character of these species (*vide infra*). The orbital term has, however, a decisive role in determining the progressively higher stability of the linear $(XeHXe^+)CO$, $(XeHXe^+)H_2O$, and $(XeHXe^+)NH_3$ with respect to the T-shaped isomers. Thus, from Table 4, while the sum ($\Delta E_{Pauli} + \Delta E_{elstat}$) of any linear isomer is invariably comparable with the corresponding term of the T-shaped isomer, the ΔE_{orb} term significantly increases in the order $N_2 < CO < H_2O < NH_3$ for the linear isomers (from -2.28 kcal mol^{-1} to -13.46 kcal mol^{-1}), but only slightly changes from -1.96 kcal mol^{-1} to -3.66 kcal mol^{-1} for the T-shaped isomers. Interestingly, if one assumes that the charge shift between $XeHXe^+$ and the ligand L occurs by orbital mixing, the relevant contribution of ΔE_{orb} to the stability of the linear $(XeHXe^+)L$ nicely parallels the higher values of Δq predicted for these complexes (see Table 2).

C. Bonding Situation by the AIM Analysis. To further scrutinize the bonding situation of the $(XeHXe^+)L$, we resorted to the AIM analysis. We based, in particular, on the joint use of numerical AIM indices, and graphic examination of the local Hamiltonian kinetic energy density, $K(\boldsymbol{r})$. In general, within the AIM analysis,[68] one explores the topology of the electron density $\rho(\boldsymbol{r})$, and calculates the value of $\rho(\boldsymbol{r})$ and

its Laplacian $\nabla^2\rho(\boldsymbol{r})$ at the (3, -1) critical points [$\nabla\rho(\boldsymbol{r}) = 0$] located on the gradient paths connecting the various bonded atoms (bond critical points, bcp's, indicated here as $\boldsymbol{r}_c$). In particular, the values of $\rho(\boldsymbol{r}_c)$ and $\nabla^2\rho(\boldsymbol{r}_c)$ allow to distinguish between covalent (shared-type) interactions, and non-covalent (closed-shell) interactions, such as ionic bonds, hydrogen bonds, and van der Waals interactions.[68] Thus, for a typical covalent bond, $\rho(\boldsymbol{r}_c)$ is relatively large and $\nabla^2\rho(\boldsymbol{r}_c) < 0$, while for a typical closed-shell interaction, $\rho(\boldsymbol{r}_c)$ is relatively small and $\nabla^2\rho(\boldsymbol{r}_c) > 0$. These criteria, however, must often contend with conflicting indications from independent evidence, and further analysis is required. In particular, Cremer and Kraka[75,76] suggested so far to relate the covalent character of a bond with the sign of the local energy density $H(\boldsymbol{r})$ at the corresponding bcp, $H(\boldsymbol{r}_c)$, $H(\boldsymbol{r})$ being the sum of the local kinetic energy density $G(\boldsymbol{r})$ (the so-called Lagrangian kinetic energy density), and the local potential energy density $V(\boldsymbol{r})$. In particular, if $\nabla^2\rho(\boldsymbol{r}_c) > 0$ but $H(\boldsymbol{r}_c) < 0$, the interaction is covalent or, at least, it possesses some degree of covalency. Complementary conditions such as $-G(\boldsymbol{r}_c)/V(\boldsymbol{r}_c) < 0.5$ and $G(\boldsymbol{r}_c)/\rho(\boldsymbol{r}_c) < 1$ were also derived.[68,77] Thus, in the AIM practice, it is customary to use the energy density $H(\boldsymbol{r})$ as a "point" index, used to catch, through the sign of $H(\boldsymbol{r}_c)$, contributing characters that escape to other indices. However, since $H(\boldsymbol{r})$ is everywhere defined as $G(\boldsymbol{r}) + V(\boldsymbol{r})$, it should signal the bonding situation not only at the bcp, but also over the entire molecular space. In particular, plotting $H(\boldsymbol{r})$ over extended regions should provide a direct visualization of the "covalent" and "non-covalent" zones of a molecular species. However, at variance with other AIM space functions such as $\rho(\boldsymbol{r})$ and $\nabla^2\rho(\boldsymbol{r})$, that are typically scrutinized in their plotted forms, the plots of $H(\boldsymbol{r})$ have received only little attention. As a matter of fact, it is practically more convenient to plot the negative energy density, $-H(\boldsymbol{r})$. This function is indeed the Hamiltonian

kinetic energy density $K(\boldsymbol{r})$, defined as $K(\boldsymbol{r}) = G(\boldsymbol{r}) - 1/4\nabla^2\rho(\boldsymbol{r})$. Plotting $K(\boldsymbol{r})$, the covalent and non-covalent regions of the molecular space are directly related, respectively, with positive and negative values of their signing function. The AIM data of $XeHXe^+$ and of the $(XeHXe^+)L$ complexes are listed in Table 5, and the plots of $K(\boldsymbol{r})$ in their main molecular planes are shown in Figure 3. In these plots, we have also included the values of $\rho(\boldsymbol{r}_c)$, $\nabla^2\rho(\boldsymbol{r}_c)$, and $K(\boldsymbol{r}_c)$ at the various bcp's.

<Table 5 and Figure 3 near here, please>

For the Xe and H atoms, the $K(\boldsymbol{r})$ plots are spherically symmetric, and the function is positive up to the outer regions. Interestingly, in the $K(\boldsymbol{r})$ plot of $XeHXe^+$ (Figure 3a), the two equivalent Xe-H bonds appear as the overlap of atomic $K(\boldsymbol{r})$ lines of positive value. Their covalent character is clearly signed by the relatively high value of $\rho(\boldsymbol{r}_c)$, 0.095 $e\ a_0^{-3}$, by the negative value of $\nabla^2\rho(\boldsymbol{r}_c)$, -0.114 $e\ a_0^{-5}$, and by the positive value of $K(\boldsymbol{r}_c)$, 0.056 hartree a_0^{-3}. In addition, from Table 5, $-G(\boldsymbol{r}_c)/V(\boldsymbol{r}_c)$ is 0.325, and $G(\boldsymbol{r}_c)/\rho(\boldsymbol{r}_c)$ is 0.284. The two bcp's fall in the "covalent" zone, whose spatial extension defines the shape of the molecular species; the covalent zone is in turn enveloped by a "non-covalent" outer region. Passing from $XeHXe^+$ to any linear $(XeHXe^+)L$, the $K(\boldsymbol{r})$ plots clearly sign the asymmetric character of the Xe1-H and the Xe-H bonds (see also Figure 1), and nicely reproduce the progressively-increased role of resonance structure **I** passing from N_2 to CO, H_2O, and NH_3 (*vide supra*). In particular, one visually notes that, compared with Xe1, the Xe atom participates to the bond with a lower number of overlapped atomic $K(\boldsymbol{r})$ lines, and tends to assume a spherical shape. This effect becomes progressively more pronounced passing from $(XeHXe^+)N_2$ (Figure 3b) to $(XeHXe^+)CO$ (Figure 3c), $(XeHXe^+)H_2O$ (Figure 3d), and $(XeHXe^+)NH_3$ (Figure 3e), and is accompanied by a progressive decrease of $\rho(\boldsymbol{r}_c)$, $\nabla^2\rho(\boldsymbol{r}_c)$, and $K(\boldsymbol{r}_c)$ at the bcp on

the Xe-H bond. In the meantime, at the bcp on the Xe1-H bond, $\rho(\boldsymbol{r}_c)$, $\nabla^2\rho(\boldsymbol{r}_c)$, and $K(\boldsymbol{r}_c)$ progressively increase. This, in general, suggests that, in a $K(\boldsymbol{r})$ plot, a covalent bond appears as the overlap of atomic $K(\boldsymbol{r})$ lines of positive value, and its strength is directly related to the number of overlapped lines. As for the interaction between $XeHXe^+$ and L, at the bcp located on the Xe1-L bond, $\rho(\boldsymbol{r}_c)$ is small, $\nabla^2\rho(\boldsymbol{r}_c)$ is invariably positive, and $-G(\boldsymbol{r}_c)/V(\boldsymbol{r}_c)$ is generally greater than 1. This suggests the essentially non-covalent character of this interaction. One notes, however, that passing from $(XeHXe^+)N_2$, to $(XeHXe^+)CO$, $(XeHXe^+)H_2O$, and $(XeHXe^+)NH_3$, $\rho(\boldsymbol{r}_c)$ progressively increases from 0.009 $e\ a_0^{-3}$ to 0.029 $e\ a_0^{-3}$, $G(\boldsymbol{r}_c)/V(\boldsymbol{r}_c)$ progressively decreases up to 0.950, and $H(\boldsymbol{r}_c)$, while generally small, decreases from 0.002 hartree a_0^{-3} to -0.001 hartree a_0^{-3}. Overall, these data suggest that, particularly in $(XeHXe^+)NH_3$, the xenon-ligand interaction has indeed some covalent contribution. Interestingly, this hint of covalency is easily caught by inspection of the $K(\boldsymbol{r}_c)$ plots. In general, the non-covalent character of the Xe-L interaction corresponds to the overalp of atomic $K(\boldsymbol{r})$ lines of negative value, the corresponding bcp falling in this "negative" region. However, passing from $(XeHXe^+)N_2$ to $(XeHXe^+)CO$, and $(XeHXe^+)H_2O$, the covalent zones of the two constituting moieties, initially well-separated, progressively approach, and, eventually, weakly overlap in $(XeHXe^+)NH_3$.

As for the T-shaped complexes, the first relevant indication from the AIM analysis is that, despite the existence of a formal connectivity between the ligand L and the H atom of $XeHXe^+$, the critical point located along this direction is indeed of the (3, +1) type (ring critical point). True bcp's were instead located on the Xe-L gradient paths. Thus, all the T-shaped $(XeHXe^+)L$ complexes must be viewed as cyclic structures, arising from the symmetric, or nearly symmetric coordination of the ligand to the Xe atoms of

$XeHXe^+$. The AIM parameters (see Table 5) are invariably suggestive of non-covalent bonds, even for L = H_2O and NH_3. This bonding situation is clearly appreciated by inspecting the $K(\boldsymbol{r})$ plots of Figure 3 (traces f-i). The two interacting moieties of the T-shaped complexes are invariably clearly recognizable as covalent zones of featuring shapes, well separated by overlapped non-covalent regions that include the Xe-L bcp's.

Finally, it is of interest to comment here on the description of the $(XeHXe^+)L$ complexes that is furnished by the criteria recently proposed by Boggs et al.[78] They examined a wide series of noble-gas molecules, and classified the interactions involving the Ng atoms into three types, namely covalent bonds, weak bonding interactions with some covalent properties (W^c), and weak bonding interactions with some non-covalent properties (W^n). A bond is covalent if the bond length agrees with the sum of the covalent atomic radii (R_{cov}), and the AIM properties at the corresponding bcp fulfill at least one of the following criteria: a) $\nabla^2\rho < 0$ and large ρ (at least 0.1 au), b) $H < 0$ and large ρ, c) $H < 0$ and $G/\rho < 1$, d) small $|H|$ (less than 0.005 au) and $G/\rho < 1$. If one or more of these criteria are fulfilled, but the bond length is longer than R_{cov}, the bond is classified as W^c; otherwise, the bond is W^n. The Xe-L distances of the $(XeHXe^+)L$ complexes (see Figures 1 and 2) are invariably longer than the sum of the covalent radii of the involved Xe, C, N, and O atoms.[79] However, for any linear and T-shaped $(XeHXe^+)L$, at the bcp of the Xe-L bond, $|H|$ is less than 0.005 au, and $G/\rho < 1$. Therefore, all these interactions are predicted to have a covalent contribution of type d). In addition, from Table 5, the Xe1-NH_3 bond of the linear $(XeHXe^+)NH_3$ (see Figure 1) features also a covalent contribution of type c) ($H < 0$ and $G/\rho < 1$). Interestingly, this is also the only interaction that, based on the joint use of AIM indices and $K(\boldsymbol{r})$ plots, is indeed predicted to have some degree of covalency (*vide supra*). Thus, at least for the

presently investigated $(XeHXe^+)L$ (L = N_2, CO, H_2O, NH_3), the Boggs' criteria probably overestimate the covalent contributions of the bonding interactions. Further work is in progress to examine the feasibility of the $K(\boldsymbol{r})$ plots to unravel the bonding situation of noble-gas compounds.

D. Harmonic Vibrational Frequencies. The MP2/aug-cc-pVTZ-PP harmonic vibrational frequencies of $XeHXe^+$ and of the $(XeHXe^+)L$ (L = N_2, CO, H_2O, NH_3) are listed in Table 6.

<Table 6 near here, please>

The symmetric mode ν_1 (152.0 cm^{-1}) and the antisymmetric mode ν_3 (943.7 cm^{-1}) of $XeHXe^+$ are higher than the experimental values of 113.7 cm^{-1} and 730.9 cm^{-1}, respectively, measured in cold matrices.[21] This discrepancy is, indeed, not unexpected. It is in fact well known that, for the $NgHNg^+$ (Ng = Ar, Kr, Xe), the major problem for the computational studies is the large difference between the predicted harmonic wavenumbers and the experimental matrix data, the theoretical values exceeding, in particular, the ν_3 wavenumbers by up to 30%.[22,24,26,27] In any case, our employed MP2 should provide a reasonable description of the effects induced on ν_1 and ν_3 by complexation. For the linear $(XeHXe^+)L$, the interaction with the ligand changes the symmetry of $XeHXe^+$ from $D_{\infty h}$ to $C_{\infty v}$ or C_{nv}, which makes the symmetric mode ν_1 IR active. The predicted absorptions are, however, only less intense, and red-shifted with respect to the naked cation. On the other hand, the most intense antisymmetric mode ν_3 is blue-shifted with respect to $XeHXe^+$. Both $\Delta\nu_1$ and $\Delta\nu_3$ progressively increase in the order N_2 < CO < H_2O < NH_3, and are, therefore, directly related to the complexation energies of the ligands (see Table 3), and to the progressively increased role of the resonance structure **I** (*vide supra*). In any case, $\Delta\nu_1$ (that ranges from -7 cm^{-1} to -76.6

cm^{-1}) is invariably significantly lower than $\Delta\nu_3$, that ranges from +53.9 cm^{-1} to +731.0 cm^{-1}. Therefore, the combination band $\nu_1 + \nu_3$ of any linear ($XeHXe^+$)L is invariably blue-shifted with respect to $XeHXe^+$ (1095.7 cm^{-1}). On the other hand, the bending mode ν_2 of $XeHXe^+$, predicted at 577.0 cm^{-1} (the experimental value is not available), is only little affected by formation of the linear complexes, with a largest blue shift of only 13.5 cm^{-1} for ($XeHXe^+$)NH_3.

For the T-shaped complexes, both the ν_1 and the ν_3 absorptions are essentially unaffected with respect to $XeHXe^+$, with minor predicted $\Delta\nu_3$ of +5.5 cm^{-1} and +6.0 cm^{-1}, respectively, for ($XeHXe^+$)N_2 and ($XeHXe^+$)CO, and of -2.1 cm^{-1} and -1.7 cm^{-1}, respectively, for ($XeHXe^+$)H_2O and ($XeHXe^+$)NH_3. On the other hand, the T-coordination removes the degeneracy of ν_2, and leads to two distinct bending absorptions, that are red- and blue-shifted, respectively, with respect to $XeHXe^+$ (577.0 cm^{-1}). The red shift is appreciable, and ranges from -10.2 cm^{-1} for ($XeHXe^+$)N_2 up to -109.3 cm^{-1} for ($XeHXe^+$)NH_3.

E. Comparison of ($XeHXe^+$)N_2 with ($ArHAr^+$)N_2 and ($KrHKr^+$)N_2. As mentioned in the Introduction, the present study was inspired also by the previous investigation of ($ArHAr^+$)N_2 and ($KrHKr^+$)N_2.[42] These species were detected by IR matrix spectroscopy, and investigated by MP2/6-311++G(2d,2p) *ab initio* calculations. At this computational level, the T-shaped isomer resulted more stable than the linear isomer by 0.8 kcal mol^{-1} for ($ArHAr^+$)N_2, and by 0.5 kcal mol^{-1} ($KrHKr^+$)N_2 (with no ZPE). In addition, the absolute complexation energies of the T-shaped isomers resulted as 3.8 kcal mol^{-1} for ($ArHAr^+$)N_2, and 3.7 kcal mol^{-1} for ($KrHKr^+$)N_2.[42] At the presently-employed CCSD(T)/aug-cc-pVTZ-PP//MP2/aug-cc-pVTZ-PP level of theory, the linear and T-shaped ($XeHXe^+$)N_2 resulted degenerate, with complexation energies of 2.8 kcal

mol^{-1} (see Table 3). While the different employed levels of theory and basis sets do not allow a direct comparison of the predicted stabilities and binding energies of the various $(NgHNg^{+})N_2$ (Ng = Ar, Kr, Xe), the absolute values (taking also into account their predicted uncertainties) are strictly similar. This suggests that, likewise $(XeHXe^{+})N_2$, both $(ArHAr^{+})N_2$ and $(KrHKr^{+})N_2$ are of mainly electrostatic character. This is also confirmed by the predicted charge transfers from N_2 to $ArHAr^{+}$ and $KrHKr^{+}$ of less than 0.001 *e*.[42]

Despite the slightly higher predicted stability of the T-shaped $(ArHAr^{+})N_2$ and $(KrHKr^{+})N_2$, the only species detected in the IR spectra were the linear isomers. In particular, their observed ν_3 resulted blue-shifted, with respect to $ArHAr^{+}$ and $KrHKr^{+}$, by 25.5 cm^{-1} and 10.4 cm^{-1}. These values revealed significantly lower than the corresponding MP2/6-311++G(2d,2p) estimates of $\Delta\nu_3$ of +68.4 cm^{-1} and +92.2 cm^{-1}, respectively, and feature also an opposite trend. Even corrected for the matrix effect, the overestimates of the experimental shifts remained as large as 32.5 cm^{-1} and 49.2 cm^{-1}, respectively.[42] For the T-shaped $(ArHAr^{+})N_2$ and $(KrHKr^{+})N_2$, the MP2/6-311++G(2d,2p) predicted, with respect to $ArHAr^{+}$ and $KrHKr^{+}$, a $\Delta\nu_3$ of -17.2 cm^{-1} and +2.5 cm^{-1}. As for the presently investigated $(XeHXe^{+})N_2$, the MP2/aug-cc-pVTZ-PP predicts a $\Delta\nu_3$ of of 53.9 cm^{-1} for the linear isomer, and of 5.5 cm^{-1} for the T-shaped isomer. Therefore, the theoretical data overall suggest an irregular periodic trend of the $\Delta\nu_3$ of the linear $(NgHNg^{+})N_2$, but a regular one for the T-shaped isomers. While these findings could invite the proposal of "chemical" explanations, the different employed basis sets, and, especially, the severe limitations of the harmonic approximation in describing the absorptions of the $NgHNg^{+}$ [22,24,26,27] warn on the quantitative relevance of these trends.

We finally note that, for $(ArHAr^+)N_2$ and $(KrHKr^+)N_2$, the missed observation of the T-shaped isomer was related to the energy barrier conceivably arising from the strong distortions of the vacancy-free fcc lattice that are needed to accommodate the nitrogen molecule in the position of the T-shaped complex.[42] Passing to $(XeHXe^+)N_2$, this shape effects could become even more pronounced. Thus, despite the predicted degeneracy of the linear and T-shaped isomers, the former should be the only detected species. It would be certainly of interest to probe this suggestion by specifically-designed experiments.

4. CONCLUSIONS

The present theoretical study revealed the ability of $XeHXe^+$ to form complexes with simple ligands. These $(XeHXe^+)L$ are thermochemically stable and, likewise the previously investigated $(ArHAr^+)N_2$ and $(KrHKr^+)N_2$,[42] they are probably observable at low temperature. The most probable candidates are the linear isomers, that arise from the coordination of L to one of the Xe atoms of $XeHXe^+$. Their formation should be signed by a blue shift of the ν_3 absorption of the naked cation, that is expected to increase by increasing the complexation energy. The observation of the T-shaped isomers, located as well as true energy minima, must probably contend with lower stability, and with the unfavorable fitting with the vacancies of the solid lattice suggested previously for the T-shaped $(ArHAr^+)N_2$ and $(KrHKr^+)N_2$.[42] We hope that our theoretical speculations could actually invite the experimental search of the $(XeHXe^+)L$. An ancillary outcome of our investigation was the suggestion of the conceivable use of the Hamiltonian kinetic energy density $K(\boldsymbol{r})$ as a probe of bonding character. Thus, for

the presently investigated ($XeHXe^+$)L, the plots of $K(\boldsymbol{r})$ naturally partition the molecular space into the "covalent" regions occupied by $XeHXe^+$ and L, and the "non-covalent" zones existing between them, and visually unravel the mainly electrostatic character of their interaction. Interestingly, for the linear ($XeHXe^+$)NH_3, the $K(\boldsymbol{r})$ plot catches also an onset of covalency in the xenon-nitrogen interaction. These findings certainly invite the further assay of $K(\boldsymbol{r})$, and its plotted forms, as a signing function of the bonding situation of noble-gas compounds.

AUTHOR INFORMATION

Corresponding Author

*E-mail: fgrandi@unitus.it

Phone: +39-0761-357126

Notes

The authors declare no competing financial interest.

ACKNOWLEDGMENTS

The authors thank the Università della Tuscia and the Italian Ministero dell'Istruzione, dell'Università e della Ricerca (MIUR) for financial support.

REFERENCES

(1) Lehmann, J.F.; Mercier, H.P.A.; Schrobilgen, G.J. The Chemistry of Krypton, *Coord. Chem. Rev.* **2002**, *233-234*, 1-39.

(2) Grochala, W. Atypical Compounds of Gases, which Have Been Called "Noble", *Chem. Soc. Rev.* **2007**, *36*, 1632-1655.

(3) Grandinetti, F. Gas-Phase Ion Chemistry of the Noble Gases: Recent Advances and Future Perspectives, *Eur. J. Mass Spectrom.* **2011**, *17*, 423-463.

(4) Hope, E.G. Coordination Chemistry of the Noble Gases and Noble Gas Fluorides, *Coord. Chem. Rev.* **2013**, *257*, 902-909.

(5) Pettersson, M.; Lundell, J.; Räsänen, M. New Rare-Gas-Containing Neutral Molecules, *Eur. J. Inorg. Chem.* **1999**, 729-737.

(6) Gerber, R.B. Formation of Novel Rare-Gas Molecules in Low-Temperature Matrices, *Annu. Rev. Phys. Chem.* **2004**, *55*, 55-78.

(7) Khriachtchev, L.; Räsänen, M.; Gerber, R.B. Noble-Gas Hydrides: New Chemistry at Low Temperatures, *Acc. Chem. Res.* **2009**, *42*, 183-191.

(8) Grochala, W.; Khriachtchev, L.; Räsänen, M. Noble-Gas Chemistry. in *Physics and Chemistry at Low Temperatures*; Khriachtchev, L., Ed.; CRC Press: 2011; pp 419-446.

(9) Khriachtchev, L.; Pettersson, M.; Runeberg, N.; Lundell, J.; Räsänen, M. A Stable Argon Compound, *Nature* **2000**, *406*, 874-876.

(10) Khriachtchev, L.; Tanskanen, H.; Lundell, J.; Pettersson, M.; Kiljunen, H.; Räsänen, M. Fluorine-Free Organoxenon Chemistry: HXeCCH, HXeCC, and HXeCCXeH, *J. Am. Chem. Soc.* **2003**, *125*, 4696-4697.

(11) Khriachtchev, L.; Isokoski, K.; Cohen, A.; Räsänen, M.; Gerber, R.B. A Small Neutral Molecule with Two Noble-Gas Atoms: HXeOXeH, *J. Am. Chem. Soc.* **2008**, *130*, 6114-6118.

(12) Arppe, T.; Khriachtchev, L.; Lignell, A.; Domanskaya, A.V.; Räsänen, M. Halogenated Xenon Cyanides ClXeCN, ClXeNC, and BrXeCN, *Inorg. Chem.* **2012**, *51*, 4398-4402.

(13) Bondybey, V.E.; Pimentel, G.C. Infrared Absorptions of Interstitial Hydrogen Atoms in Solid Argon and Krypton, *J. Chem. Phys.* **1972**, *56*, 3832-3836.

(14) Beyer, M.; Lammers, A.; Savchenko, E.V.; Niedner-Schatteburg, G.; Bondybey, V.E. Proton Solvated by Noble-Gas Atoms: Simplest Case of a Solvated Ion, *Phys. Chem. Chem. Phys.* **1999**, *1*, 2213-2221.

(15) Beyer, M.; Savchenko, E.V.; Niedner-Schatteburg, G.; Bondybey, V.E. Diffusion of Hydrogen in Rare Gas Solids: Neutral H Atoms and H^+ Protons, *Low Temp. Phys.* **1999**, *25*, 814-817.

(16) Beyer, M.K.; Bondybey, V.E.; Savchenko, E.V. The Contribution of Tunneling to the Diffusion of Protons and Deuterons in Rare Gas Solids, *Low Temp. Phys.* **2003**, *29*, 792-794.

(17) Savchenko, E.V.; Khyzhniy, I.V.; Uyutnov, S.A.; Gumenchuk, G.B.; Ponomaryov, A.N.; Beyer, M.K.; Bondybey, V.E. Formation of $(Xe_2H)^*$ Centers in Solid Xe via Recombination: Nonstationary Luminescence and Internal Electron Emission, *Low Temp. Phys.* **2010**, *36*, 407-410.

(18) Milligan, D.E.; Jacox, M.E. Infrared Spectroscopic Evidence for the Stabilization of HAr_n^+ in Solid Argon at 14 K, *J. Mol. Spectrosc.* **1973**, *46*, 460-469.

(19) Andrews, L.; Ault, B.S.; Grzybowski, J.M.; Allen, R.O. Proton and Deuteron Radiolysis of Argon Matrix Samples of O_2 and Cl_2. Infrared Spectra of Charged Species, *J. Chem. Phys.* **1975**, *62*, 2461-2464.

(20) Wight, C.A.; Ault, B.S.; Andrews, L. On Microwave Discharge Sources of New Chemical Species for Matrix-Isolation Spectroscopy and the Identification of Charged Species, *J. Chem. Phys.* **1976**, *65*, 1244-1249.

(21) Kunttu, H.; Seetula, J.; Räsänen, M.; Apkarian, V.A. Photogeneration of Ions via Delocalized Charge Transfer States. I. Xe_2H^+ and Xe_2D^+ in Solid Xenon, *J. Chem. Phys.* **1992**, *96*, 5630-5635.

(22) Nieminen, J.; Kauppi, E.; Lundell, J.; Kunttu, H. Potential Energy Surface and Vibrational Analysis Along the Stretching Vibrations of $XeHXe^+$ Ion, *J. Chem. Phys.* **1993**, *98*, 8698-8703.

(23) Kunttu, H.M.; Seetula, J.A. Photogeneration of Ionic Species in Ar, Kr and Xe Matrices Doped with HCl, HBr and HI, *Chem. Phys.* **1994**, *189*, 273-292.

(24) Lundell, J.; Kunttu, H. Structure, Spectra, and Stability of Argon Hydride Ion (Ar_2H^+), Krypton Hydride Ion (Kr_2H^+), Xenon Hydride Ion (Xe_2H^+): an Effective Core Potential Approach, *J. Phys. Chem.* **1992**, *96*, 9774-9781.

(25) Nieminen, J.; Kauppi, E. Potential Energy Surface and Vibrational Analysis Along the Stretching Vibrations of the $ArHAr^+$ Ion, *Chem. Phys. Lett.* **1994**, *217*, 31-35.

(26) Lundell, J. Density Functional Approach on Ground State RgH^+ and $RgHRg^+$ (Rg = Ar, Kr, Xe) Ions, *J. Mol. Struct.* **1995**, *355*, 291-297.

(27) Lundell, J.; Pettersson, M.; Räsänen, M. The Proton-Bound Rare Gas Compounds $(RgHRg')^+$ (Rg = Ar, Kr, Xe) - A Computational Approach, *Phys. Chem. Chem. Phys.* **1999**, *1*, 4151-4155.

(28) Lundell, J.; Pettersson, M. Molecular Properties of $Xe_2H_3^+$, *J. Mol. Struct.* **1999**, *509*, 49-54.

(29) Lundell, J.; Berski, S.; Latajka, Z. Density Functional Study of the $Xe_2H_3^+$ Cation, *Chem. Phys.* **1999**, *247*, 215-224.

(30) Khriachtchev, L.; Lignell, A.; Rasanen, M. Neutralization of Solvated Protons and Formation of Noble-Gas Hydride Molecules: Matrix-Isolation Indications of Tunneling Mechanisms?, *J Chem. Phys.* **2005**, *123*, 64507.

(31) Tanskanen, H.; Khriachtchev, L.; Lignell, A.; Räsänen, M.; Johansson, S.; Khyzhniy, I.; Savchenko, E. Formation of Noble-Gas Hydrides and Decay of Solvated Protons Revisited: Diffusion-Controlled Reactions and Hydrogen Atom Losses in Solid Noble Gases, *Phys. Chem. Chem. Phys.* **2008**, *10*, 692-701.

(32) Fridgen, T.D.; Parnis, J.M. Electron Bombardment Matrix Isolation of Rg/Rg'/Methanol Mixtures (Rg = Ar, Kr, Xe): Fourier-Transform Infrared Characterization of the Proton-Bound Dimers Kr_2H^+, Xe_2H^+, $(ArHKr)^+$ and $(ArHXe)^+$ in Ar Matrixes and $(KrHXe)^+$ and Xe_2H^+ in Kr Matrices, *J. Chem. Phys.* **1998**, *109*, 2155-2161.

(33) Fridgen, T.D., Parnis, J.M., Density Functional Theory Study of the Proton-Bound Rare-Gas Dimers Rg_2H^+ and $(RgHRg')^+$ (Rg = Ar, Kr, Xe): Interpretation of Experimental Matrix Isolation Infrared Data, *J. Chem. Phys.* **1998**, *109*, 2162-2168.

(34) Rosenkrantz, M.E. Ab Initio Study of ArH, ArH^+, Ar_2H, Ar_2H^+, and Ar_4H^+, *Chem. Phys. Lett.* **1990**, *173*, 378-383.

(35) Last, I.; George, T.F. Semiempirical Study of Rare Gas and Rare Gas-Hydrogen Ionic Clusters: R_n^+, $(R_nH)^+$, and $(R_nH_2)^+$ for R = Ar, Xe, *J. Chem. Phys.* **1990**, *93*, 8925-8938.

(36) Filippone, F.; Gianturco, F.A. Simulating Ionic Microsolvation: Protonated Argon Clusters, *Phys. Chem. Chem. Phys.* **1999**, *1*, 5537-5545.

(37) Qu, J.Y.; Li, W.; Guo, R.; Zhao, X.S. A Global Potential Energy Surface of Ar_2H^+ Based on *Ab Initio* Calculations, *J. Chem. Phys.* **2002**, *117*, 2592-2598.

(38) Li, W.; Zhao, X.S. Theoretical Prediction on Vibrational Spectra of $[Ar\cdots Ar\text{-}H]^+$, *Science China B* **2003**, *46*, 321-329.

(39) Giju, K.T.; Roszak, S.; Leszczynski, J. A Theoretical Study of Protonated Argon Clusters: Ar_nH^+(n = 1-7), *J. Chem. Phys.* **2002**, *117*, 4803-4809.

(40) Ritschel, T.; Zuelicke, L.; Kuntz, P.J. Cationic van-der-Waals Complexes: Theoretical Study of Ar_2H^+ Structure and Stability, *Z. Phys. Chem.* **2004**, *218*, 377-390.

(41) Borocci, S.; Giordani, M.; Grandinetti, F. Cationic Noble Gas Hydrides-2: A Theoretical Investigation on $HNgHNgH^+$ (Ng = Ar, Kr, Xe), *Comput. Theor. Chem.* **2011**, *964*, 318-323.

(42) Lignell, A.; Khriachtchev, L.; Lignell, H.; Räsänen, M. Protons Solvated in Noble-Gas Matrices: Interaction with Nitrogen, *Phys. Chem. Chem. Phys.* **2006**, *8*, 2457-2463.

(43) Frisch, M.J.; Trucks, G.W.; Schlegel, H.B.; Scuseria, G.E.; Robb, M.A.; Cheeseman, J.R.; Montgomery, Jr., J.A.; Vreven, T.; Kudin, K.N.; Burant, J.C. et al. *Gaussian 03*, revision D.02; Gaussian, Inc.: Wallington, CT, 2004.

(44) Møller, C.; Plesset, M.S. Note on the Approximation Treatment for Many-Electrons Systems, *Phys. Rev.* **1934**, *46*, 618-622.

(45) Raghavachari, K.; Trucks, G.W.; Pople, J.A.; Head-Gordon, M. A Fifth-Order Perturbation Comparison of Electron Correlation Theories. *Chem. Phys. Lett.* **1989**, *157* 479-483.

(46) Peterson, K.A.; Figgen, D.; Goll, E.; Stoll, H.; Dolg, M. Systematically Convergent Basis Sets with Relativistic Pseudopotentials. II. Small-Core Pseudopotentials and Correlation Consistent Basis Sets for the Post-*d* Group 16-18 Elements, *J. Chem. Phys.* **2003**, *119*, 11113-11123.

(47) Kendall, R.A.; Dunning, T.H., Jr.; Harrison, R.J. Electron Affinities of the First-Row Atoms Revisited. Systematic Basis Sets and Wave Functions, *J. Chem. Phys.* **1992**, *96*, 6796-6806.

(48) Boys, S.; Bernardi, F. The Calculation of Small Molecular Interactions by the Differences of Separate Total Energies. Some Procedures with Reduced Errors, *Mol. Phys.* **1970**, *19*, 553-566.

(49) Glendening, E.D.; Weinhold, F. Natural Resonance Theory: I. General Formalism, *J. Comput. Chem.* **1998**, *19*, 593-609.

(50) Glendening, E.D.; Weinhold, F. Natural Resonance Theory: II. Natural Bond Order and Valency, *J. Comput. Chem.* **1998**, *19*, 610-627.

(51) Glendening, E.D.; Badenhoop, J.K.; Weinhold, F. Natural Resonance Theory: III. Chemical Applications, *J. Comput. Chem.* **1998**, *19*, 628-646.

(52) Weinhold, F. Natural Bond Orbital Analysis: a Critical Overview of Relationships to Alternative Bonding Perspectives, *J. Comput. Chem.* **2012**, *33*, 2363-2379, and references therein.

(53) Glendening, E.D.; Badenhoop, J.K.; Reed, A.E.; Carpenter, J.E.; Bohmann, J.A.; Morales, C.M.; Landis, C.R.; Weinhold, F. *NBO 6.0*; Theoretical Chemistry Institute, University of Wisconsin: Madison, 2013.

(54) Ziegler, T.; Rauk, A. On the Calculation of Bonding Energies by the Hartree Fock Slater Method. I. The Transition State Method, *Theor. Chim. Acta* **1977**, *46*, 1-10.

(55) Ziegler, T.; Rauk, A. A Theoretical Study of the Ethylene-Metal Bond in Complexes between Cu^+, Ag^+, Au^+, Pt^0 or Pt^{2+} and Ethylene, based on the Hartree-Fock-Slater Transition-State Method, *Inorg. Chem.* **1979**, *18*, 1558-1565.

(56) Ziegler, T.; Rauk, A. CO, CS, N_2, PF_3, and $CNCH_3$ as σ Donors and π Acceptors. A Theoretical Study by the Hartree-Fock-Slater Transition-State Method, *Inorg. Chem.* **1979**, *18*, 1755-1758.

(57) *ADF2012*, *SCM*; Theoretical Chemistry, Vrije Universiteit: Amsterdam, The Netherlands, http://www.scm.com.

(58) te Velde, G.; Bickelhaupt, F.M.; van Gisbergen, S.J.A.; Fonseca Guerra, C.; Baerends, E.J.; Snijders, J.G.; Ziegler, T. Chemistry with ADF, *J. Comput. Chem.* **2001**, *22*, 931-967.

(59) Fonseca Guerra, C.; Snijders, J.G.; te Velde, G.; Baerends, E.J. Towards an Order-N DFT Method, *Theor. Chem. Acc.* **1998**, *99*, 391-403.

(60) Becke, A.D. Density-Functional Exchange-Energy Approximation with Correct Asymptotic Behaviour, *Phys. Rev. A* **1988**, *38*, 3098-3100.

(61) Becke, A.D. Density-Functional Thermochemistry. III. The Role of Exact Exchange, *J. Chem. Phys.* **1993**, *98*, 5648-5652.

(62) Lee, C.; Yang, W.; Parr, R.G. Development of the Colle-Salvetti Correlation-Energy Formula into a Functional of the Electron Density, *Phys. Rev. B* **1988**, *37*, 785-789.

(63) Grimme, S.; Jens, A.; Ehrlich, S.; Krieg, H. A Consistent and Accurate *ab initio* Parametrization of Density Functional Dispersion Correction (DFT-D) for the 94 Elements H-Pu, *J. Chem. Phys.* **2010**, *132*, 154104.

(64) van Lenthe, E.; Baerends, E.J. Optimized Slater-Type Basis Sets for the Elements 1-118, *J. Comput. Chem.* **2003**, *24*, 1142-1156.

(65) Baerends, E.J.; Ellis, D.E.; Ros, P. Self-Consistent Molecular Hartree-Fock-Slater Calculations I. The Computational Procedure, *Chem. Phys.* **1973**, *2*, 41-51.

(66) Krijn, J.; Baerends, E.J. Fit-Functions in the HFS method; Internal Report, Vrije Universiteit: Amsterdam, 1984.

(67) van Lenthe, E.; Ehlers, A.E.; Baerends, E.J. Geometry Optimization in the Zero Order Regular Approximation for Relativistic Effects, *J. Chem. Phys.* **1999**, *110*, 8943-8954.

(68) Bader, R.F.W. *Atoms in Molecules: a Quantum Theory*; Oxford University Press: Oxford, 1990.

(69) Keith, T.A. *AIMAll*, Version 12.11.09; TK Gristmill Software: Overland Park KS, USA, 2012. http://aim.tkgristmill.com.

(70) Keith, T.A.; Frisch, M.J. Subshell Fitting of Relativistic Atomic Core Electron Densities for Use in QTAIM Analyses of ECP-based Wave Functions, *J. Phys. Chem. A* **2011**, *115*, 12879-12894.

(71) Pimentel, G.C. The Bonding of Trihalide and Bifluoride Ions by the Molecular Orbital Method, *J. Chem. Phys.* **1951**, *19*, 446-448.

(72) Landis, C.R.; Weinhold, F. 3c/4e σ-Type Long-Bonding: A Novel Transitional Motif toward the Metallic Delocalization Limit, *Inorg. Chem.* **2013**, *52*, 5154-5166.

(73) For the N_2 and CO ligands, we reoptimized the geometries of the two isomers at the CCSD(T)/aug-cc-pVDZ level of theory, and used these structures to calculate their binding energies at the CCSD(T)/aug-cc-pVTZ level of theory. The obtained values

resulted, however, essentially unchanged, and it is, therefore, not possible to definitely conclude on the relative stability of the linear and T-shaped isomers.

(74) Jamshidi, Z.; Eskandari, K.; Azami, S.M. Nature of Closed- and Open-Shell Interactions between Noble Metals and Rare Gas Atoms, *Int. J. Quantum Chem.* **2013**, *113*, 1981-1991.

(75) Cremer, D.; Kraka, E. Chemical Bonds without Bonding Electron Density - Does the Difference Electron-Density Analysis Suffice for a Description of the Chemical Bond?, *Angew. Chem. Int. Ed. Engl.* **1984**, *23*, 627-628.

(76) Cremer, D.; Kraka, E. A Description of the Chemical Bond in Terms of Local Properties of Electron Density and Energy, *Croat. Chem. Acta* **1984**, *57*, 1259-1281.

(77) Ziółkowski, M.; Grabowski, S.J.; Leszczynski, J. Cooperativity in Hydrogen-Bonded Interactions: Ab Initio and "Atoms in Molecules" Analyses, *J. Phys. Chem. A* **2006**, *110*, 6514-6521.

(78) Zou, W.; Nori-Shargh, D.; Boggs, J. On the Covalent Character of Rare Gas Bonding Interactions: A New Kind of Weak Interaction, J. *Phys. Chem. A* **2013**, *117*, 207-212.

(79) Pyykkö, P.; Atsumi, M. Molecular Single-Bond Covalent Radii for Elements 1-118, *Chem. Eur. J.* **2009**, *15*, 186-197.

Table 1. MP2/aug-cc-pVTZ-PP NRT Percentage Contributions of the (Xe)(H-Xe1$^+$)(L) and (Xe-H$^+$)(Xe1)(L) Resonance Structures I and II (see also Figure 1) of the Linear (XeHXe$^+$)L Complexes

L	**I**	**II**	BO[a] (Xe-H)			BO[a] (Xe1-H)		
None	50.0	50.0	0.500	0.230 (46.0%)	0.270 (54.0%)			
N_2	55.5	43.1	0.431	0.175 (40.6%)	0.256 (59.4%)	0.555	0.285 (51.4%)	0.270 (48.6%)
CO	59.1	39.7	0.397	0.147 (37.0%)	0.249 (63.0%)	0.591	0.320 (54.1%)	0.271 (45.9%)
H_2O	69.1	26.7	0.267	0.079 (29.6%)	0.189 (70.4%)	0.691	0.428 (61.9%)	0.263 (38.1%)
NH_3	74.9	19.0	0.190	0.041 (21.6%)	0.148 (78.4%)	0.749	0.501 (66.9%)	0.248 (33.1%)

[a] NRT Bond Order (total/covalent/ionic).

Table 2. MP2/aug-cc-pVTZ-PP NBO atomic charges (*e*) of the ($XeHXe^+$)L complexes (see Figures 1 and 2)

	L	*q*(H)	*q*(Xe)	*q*(Xe1)	*q*(L)		Δq[a]
	None	0.094	0.453				
Linear	N_2	0.093	0.395	0.510	-0.071 (N1)	0.073 (N2)	0.002
	CO	0.093	0.360	0.537	0.375 (C)	-0.365 (O)	0.010
	H_2O	0.103	0.264	0.621	-0.974 (O)	0.493 (H1)	0.012
	NH_3	0.102	0.186	0.660	-1.094 (N)	0.382 (H1)	0.052
T-shaped	N_2	0.098	0.452		-0.076 (N1)	0.074 (N2)	-0.002
	CO	0.099	0.451		0.367 (C)	-0.368 (O)	-0.001
	H_2O	0.104	0.448		-0.970 (O)	0.485 (H1)	0.000
	NH_3	0.109	0.435	0.452	-1.100 (N)	0.368 (H1)	0.004
						0.368 (H2)	
						0.368 (H3)	

[a] Shift of Charge from L to $XeHXe^+$.

Table 3. CCSD(T)/aug-cc-pVTZ-PP//MP2/aug-cc-pVTZ-PP dissociation energies (kcal mol^{-1}) of the (XeHXe^{+})L complexes (see Figures 1 and 2)

	L	ΔE_{el}	ΔE_0	ΔE_0 (BSSE)
Linear	N_2	2.8	2.3	2.0
	CO	4.0	3.3	2.8
	H_2O	12.0	10.4	10.0
	NH_3	15.7	13.2	12.7
T-shaped	N_2	2.8	2.4	2.0
	CO	3.5	3.1	2.6
	H_2O	11.0	9.9	9.4
	NH_3	11.2	10.2	9.7

Table 4. B3LYP-D3/TZ2P EDA Analysis of the Interaction between $XeHXe^+$ and L in the $(XeHXe^+)L$ Complexes (see Figures 1 and 2)

	L	ΔE_{prep}	ΔE_{Pauli}	ΔE_{elstat}[a]	ΔE_{orb}[a]	ΔE_{disp}[a]	ΔE
Linear	N_2	0.29	2.57	-2.31 (42.0)	-2.28 (41.5)	-0.91 (16.5)	-2.64
	CO	0.35	4.12	-4.07 (50.0)	-3.11 (38.2)	-0.96 (11.8)	-3.67
	H_2O	1.24	11.05	-16.37 (70.6)	-6.05 (26.1)	-0.76 (3.3)	-10.89
	NH_3	2.86	22.79	-26.23 (63.9)	-13.46 (32.8)	-1.39 (3.3)	-15.43
T-shaped	N_2	0.20	2.48	-1.83 (33.2)	-1.96 (35.6)	-1.72 (31.2)	-2.83
	CO	0.12	2.88	-2.58 (40.1)	-2.00 (31.0)	-1.86 (28.9)	-3.44
	H_2O	0.36	6.60	-12.65 (73.0)	-2.69 (15.5)	-1.99 (11.5)	-10.37
	NH_3	0.76	8.10	-13.24 (68.3)	-3.66 (18.9)	-2.48 (12.8)	-10.52

[a] The Value in Parenthesis is the Percentage Contribution to the Attractive Part of ΔE ($\Delta E_{elstat} + \Delta E_{orb} + \Delta E_{disp}$).

Table 5. MP2/aug-cc-pVTZ-PP AIM data[a] of the ($XeHXe^+$)L complexes (see Figures 1 and 2)

	L	bond	ρ	$\nabla^2\rho$	K	H	G	V	$-G/V$	G/ρ
	None	Xe-H	0.095	-0.114	0.056	-0.056	0.027	-0.083	0.325	0.284
Linear	N_2	Xe-H	0.082	-0.068	0.043	-0.043	0.026	-0.069	0.377	0.317
		Xe1-H	0.108	-0.163	0.070	-0.070	0.029	-0.099	0.293	0.268
		Xe1-N1	0.009	0.032	-0.002	0.002	0.007	-0.005	1.400	0.778
	CO	Xe-H	0.074	-0.044	0.035	-0.035	0.025	-0.060	0.417	0.338
		Xe1-H	0.116	-0.191	0.078	-0.078	0.030	-0.108	0.278	0.259
		Xe1-C	0.011	0.033	-0.001	0.001	0.007	-0.006	1.167	0.636
	H_2O	Xe-H	0.055	0.008	0.019	-0.019	0.021	-0.040	0.525	0.382
		Xe1-H	0.136	-0.265	0.100	-0.100	0.034	-0.134	0.254	0.250
		Xe1-O	0.021	0.082	-0.002	0.002	0.018	-0.016	1.125	0.857
	NH_3	Xe-H	0.041	0.034	0.010	-0.010	0.018	-0.028	0.643	0.439
		Xe1-H	0.147	-0.294	0.112	-0.112	0.038	-0.150	0.253	0.258
		Xe1-N	0.029	0.076	0.001	-0.001	0.019	-0.020	0.950	0.655
T-shaped	N_2	Xe-H	0.095	-0.115	0.056	-0.056	0.027	-0.083	0.325	0.284
		Xe-N1	0.006	0.019	-0.001	0.001	0.004	-0.003	1.333	0.667
	CO	Xe-H	0.095	-0.116	0.056	-0.056	0.027	-0.083	0.325	0.284
		Xe-C	0.006	0.018	-0.001	0.001	0.003	-0.002	1.500	0.500
	H_2O	Xe-H	0.095	-0.117	0.056	-0.056	0.027	-0.083	0.325	0.284
		Xe-O	0.010	0.033	-0.001	0.001	0.007	-0.006	1.167	0.700
	NH_3	Xe-H	0.097	-0.125	0.058	-0.058	0.027	-0.085	0.318	0.278
		Xe1-H	0.093	-0.109	0.054	-0.054	0.026	-0.080	0.325	0.280
		Xe-N	0.010	0.028	-0.001	0.001	0.006	-0.005	1.200	0.600
		Xe1-N	0.010	0.028	-0.001	0.001	0.006	-0.005	1.200	0.600

[a] The charge density ρ ($e\ a_0^{-3}$), the Laplacian of the charge density $\nabla^2\rho$ ($e\ a_0^{-5}$), the Hamiltonian kinetic energy density K (hartree a_0^{-3}), the energy density H (hartree a_0^{-3}), the Lagrangian kinetic energy density G (hartree a_0^{-3}), and the potential energy density V (hartree a_0^{-3}) are calculated at the charge-density critical point ($\nabla\rho = 0$) on the specified bond.

Table 6. MP2/aug-cc-pVTZ-PP harmonic vibrational frequencies (cm^{-1}) of the ($XeHXe^{+}$)L complexes (see Figures 1 and 2). ν_1 is the symmetric mode, ν_2 is the bending mode, and ν_3 is the antisymmetric mode. Δ is the vibrational frequency shift upon complexation. The IR absorption intensities (km mol^{-1}) are given in parentheses

	L	ν_1	ν_2	ν_3	$\Delta\nu_3$	$\nu_1 + \nu_3$	$\Delta(\nu_1 + \nu_3)$
	None	152.0 (0)	577.0 (3.1)[a]	943.7 (7060.9)	-	1095.7	
Linear	N_2	143.0 (29.6)	587.9 (3.4)[a]	997.6 (7388.9)	+53.9	1140.6	+44.9
	CO	130.5 (51.1)	589.3 (3.8)[a]	1075.7 (7212.4)	+132.0	1206.2	+110.5
	H_2O	97.8 (52.9)	569.6 (5.9)/577.7 (1.5)	1396.2 (5446.9)	+452.5	1494.0	+398.3
	NH_3	75.4 (42.6)	590.5 (0.3)[a]	1674.7 (3347.0)	+731.0	1750.1	+654.4
T-shaped	N_2	152.1 (0.0_3)	566.8 (6.3)/579.0 (2.5)	949.2 (6796.3)	+5.5	1101.3	+5.6
	CO	151.9 (0.0_4)	561.7 (6.7)/579.8 (2.3)	949.7 (6699.3)	+6.0	1101.6	+5.9
	H_2O	152.0 (0.2)	536.6 (9.6)/591.1 (3.4)	941.6 (6932.4)	-2.1	1093.6	-2.1
	NH_3	149.4 (0.2)	467.7 (16.6)/594.2 (3.5)	942.0 (6688.1)	-1.7	1091.4	-4.3

[a] Doubly degenerate.

Captions for Figures

Figure 1. MP2/aug-cc-pVTZ-PP optimized geometries (Å and °) of $XeHXe^+$ and of the linear $(XeHXe^+)L$ (L = N_2, CO, H_2O, NH_3).

Figure 2. MP2/aug-cc-pVTZ-PP optimized geometries (Å and °) of the T-shaped $(XeHXe^+)L$ (L = N_2, CO, H_2O, NH_3).

Figure 3. Plot of the MP2/aug-cc-pVTZ-PP Hamiltonian kinetic energy density $K(\boldsymbol{r})$ in the molecular plane of $XeHXe^+$ and of the linear and T-shaped $(XeHXe^+)L$ (L = N_2, CO, H_2O, NH_3). The bold lines mark the separation between the regions of positive (inner) and negative (outer) values of $K(\boldsymbol{r})$. The quoted numbers are (from top to bottom) the values of $\rho(\boldsymbol{r})$ ($e\ a_0^{-3}$), $\nabla^2\rho(\boldsymbol{r})$ ($e\ a_0^{-5}$), and $K(\boldsymbol{r})$ (hartree a_0^{-3}) at the (3, -1) critical points on the Xe-H and Xe-L bond paths.

Figure 1

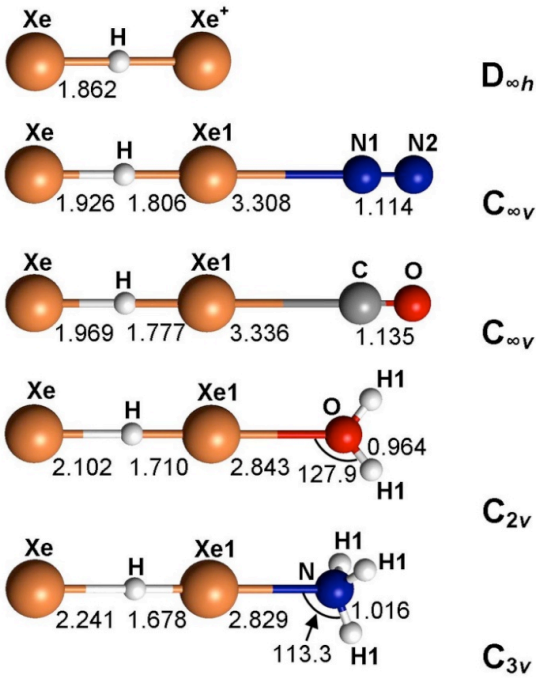
Xe
H
Xe+
1.862
D∞h
Xe
H
Xe1
N1
N2
1.926
1.806
3.308
1.114
C∞v
Xe
H
Xe1
C
O
1.969
1.777
3.336
1.135
C∞v
Xe
H
Xe1
O
H1
0.964
2.102
1.710
2.843
127.9
H1
C2v
Xe
H
Xe1
N
H1
H1
1.016
2.241
1.678
2.829
113.3
H1
C3v

Figure 2

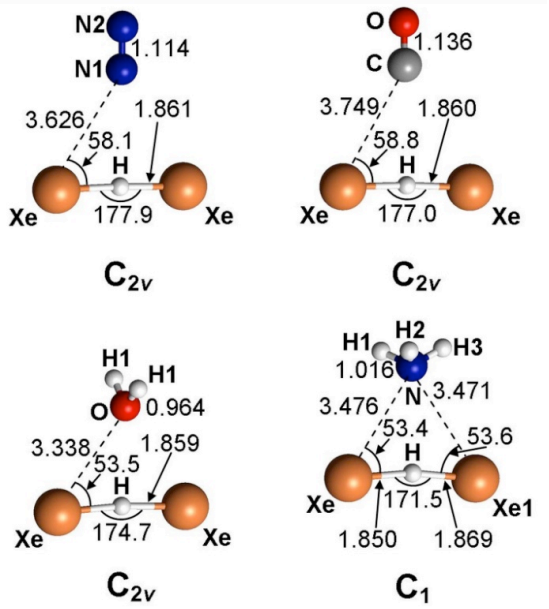
N2
1.114
N1
3.626
1.861
58.1
H
Xe
177.9
Xe
C2v
O
1.136
C
3.749
1.860
58.8
H
Xe
177.0
Xe
C2v
H1
H1
O
0.964
3.338
1.859
53.5
H
Xe
174.7
Xe
C2v
H1
H2
H3
1.016
N
3.471
3.476
53.4
53.6
H
Xe
171.5
Xe1
1.850
1.869
C1

Figure 3

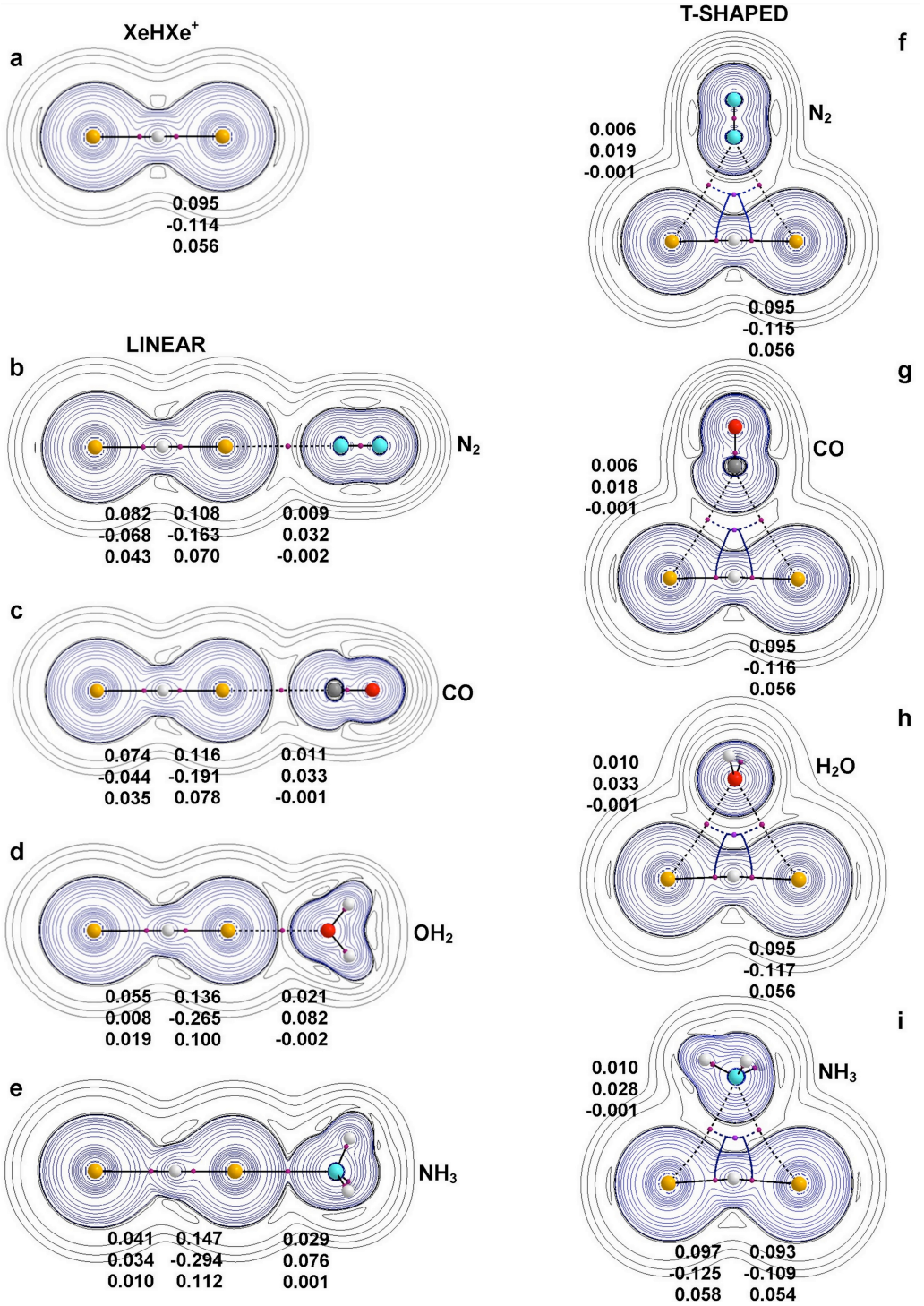
XeHXe+
a
0.095
-0.114
0.056
LINEAR
b
N2
0.082 0.108 0.009
-0.068 -0.163 0.032
0.043 0.070 -0.002
c
CO
0.074 0.116 0.011
-0.044 -0.191 0.033
0.035 0.078 -0.001
d
OH2
0.055 0.136 0.021
0.008 -0.265 0.082
0.019 0.100 -0.002
e
NH3
0.041 0.147 0.029
0.034 -0.294 0.076
0.010 0.112 0.001
T-SHAPED
f
N2
0.006
0.019
-0.001
0.095
-0.115
0.056
g
CO
0.006
0.018
-0.001
0.095
-0.116
0.056
h
H2O
0.010
0.033
-0.001
0.095
-0.117
0.056
i
NH3
0.010
0.028
-0.001
0.097 0.093
-0.125 -0.109
0.058 0.054

TOC